Coupled constitutive relations: A second law based higher order closure for hydrodynamics

Anirudh Singh Rana[1], Vinay Kumar Gupta*[2], and Henning Struchtrup[3]

[1]*Institute of Advanced Study, University of Warwick, Coventry CV4 7HS, UK*
[1,2]*Mathematics Institute, University of Warwick, Coventry CV4 7AL, UK*
[2]*Department of Mathematics, SRM Institute of Science and Technology, Chennai 603203, India*
[3]*Department of Mechanical Engineering, University of Victoria, Victoria, British Columbia V8W 2Y2, Canada*

Abstract

In the classical framework, the Navier–Stokes–Fourier equations are obtained through the linear uncoupled thermodynamic force-flux relations which guarantee the non-negativity of the entropy production. However, the conventional thermodynamic description is only valid when the Knudsen number is sufficiently small. Here, it is shown that the range of validity of the Navier–Stokes–Fourier equations can be extended by incorporating the nonlinear coupling among the thermodynamic forces and fluxes. The resulting system of conservation laws closed with the coupled constitutive relations is able to describe many interesting rarefaction effects, such as Knudsen paradox, transpiration flows, thermal stress, heat flux without temperature gradients, etc., which can not be predicted by the classical Navier–Stokes–Fourier equations. For this system of equations, a set of phenomenological boundary conditions, which respect the second law of thermodynamics, is also derived. Some of the benchmark problems in fluid mechanics are studied to show the applicability of the derived equations and boundary conditions.

1 Introduction

The classical Navier–Stokes–Fourier (NSF) equations are known to fail in describing small-scale flows, for which the Knudsen number—defined as the ratio of the molecular mean free path to a characteristic hydrodynamic length scale—is sufficiently large [1, 2]. It is well established that the traditional NSF equations cannot describe strong non-equilibrium effects, which occur at high Knudsen numbers; for instance, the classical NSF equations are not able to describe the heat flux parallel to flow direction which is not forced by temperature gradient [3, 4], nonuniform pressure profile and characteristic temperature dip in Poiseuille flow [5–7], non-Fourier heat flux in a lid-driven cavity where heat flows from low temperature to high temperature [8, 9], etc.

Several approaches to irreversible thermodynamics are available to determine the properties of a system near equilibrium. Linear Irreversible Thermodynamics (LIT) [10, 11] is based on the assumption of *local thermodynamic equilibrium*, where thermal and caloric state equation and the Gibbs equation locally retain the forms they have in equilibrium. Gibbs equation and conservation laws for mass, momentum and energy are then combined to derive a mathematical form of the second law of thermodynamics–the balance equation for entropy. The requirement of positivity of the entropy generation rate leads directly to the constitutive laws for stress tensor and heat flux, resulting in the well-known laws of Navier–Stokes and Fourier [12, 13].

*Corresponding author (✉ vinay.gupta@warwick.ac.uk)

Rational Thermodynamics (RT) [14], in an attempt to relax the requirement of local thermodynamic equilibrium, postulates a particular form of the balance law for entropy, the Clausius–Duhem equation. Here, the non-convective entropy flux is prescribed to be the heat flux divided by the thermodynamic temperature—a relation that is one of the results of LIT. A careful evaluation of the conservation laws together with the entropy equation results in constitutive equations for stress tensor and heat flux. For simple fluids, RT gives the same constitutive equations as LIT, including the relations that describe local thermodynamic equilibrium [13].

Hence, although their postulates differ, both approaches—LIT and RT—appear to be equivalent for simple fluids. A particular feature of both approaches is the form of the entropy generation rate as the sum of products of thermodynamic forces and thermodynamic fluxes. The forces describe deviation from global thermodynamic equilibrium, and typically are gradients, e.g., those of temperature and velocity. The fluxes, e.g., heat flux and stress tensor, describe processes that aim to reduce the forces. For processes that are not too far from equilibrium, as described by LIT and RT, forces and fluxes are mathematically uncoupled, in the sense that the fluxes do not appear in the expressions for the forces.

The increasing miniaturization of physical devices has directed attention to the strong non-equilibrium conditions where the classical equations derived by LIT and RT loose their validity, and must be enhanced by proper extensions of the methods of derivation. In the present contribution, considering rarefied gas flows, we present an enhancement, based on a correction of the entropy flux that is suggested from the Kinetic Theory of Gases and Extended Thermodynamics [15].

A detailed description of a gas flow, ranging from near equilibrium to strong non-equilibrium conditions, is offered by the Boltzmann equation, which solves for the microscopic distribution function of gas molecules [16]. However, being a nonlinear integro-differential equation, the Boltzmann equation is difficult to solve and its direct solutions are computationally expensive. An alternative, but complementary, modeling of a gas can be done through macroscopic description, in which the behavior of a gas is described by moments of the distribution function [2, 17]. The main aim of the macroscopic modeling is to reduce the complexity by considering the transport equations for a finite number of (low-dimensional) moments—referred to as moment equations—instead of solving the Boltzmann equation for the (high-dimensional) distribution function. It is worth to note that the physical quantities, such as density, temperature, velocity, stress tensor and heat flux, in a gas appear as moments of the distribution function. Moment equations form an open hierarchy of equations, thus requiring a suitable closure. In kinetic theory, there are many approximation methods for closing a set of moment equations [17]. The well-known approximation methods include the Hilbert expansion method [1], the Chapman–Enskog (CE) expansion method [18], the Grad's moment method [19], regularized moment method[20, 21], and entropy maximization [22, 23].

The CE expansion method relies on the smallness of the Knudsen number. At zeroth- and first-order approximations the method leads to the Euler and NSF equations, and is fully equivalent to the results of LIT and RT (local equilibrium, etc.). At the second- and third-order approximations the method yields the the Burnett and super-Burnett equations, respectively, which exhibit instabilities for time-dependent problems [24], and are thermodynamically inconsistent [25, 26]. During the last decade, several modified forms of the Burnett equations have been suggested in the literature, see e.g. [27–30], that are stable; however, at present no proper boundary conditions are available for any of these sets of equations, hence their applicability is limited. On the other hand, linearized Grad's 13 (also R13) moment equations comply with the second law of thermodynamics, which also leads to thermodynamically consistent boundary conditions for these set of equations [31]. However, no entropy law has been established for the nonlinear moment equations.

In the following, we propose a phenomenological procedure in which the entropy flux contains a nonlinear contribution in stress and heat flux, which is motivated by results from Rational

Extended Thermodynamics (RET) [15]. In contrast to RET, where, similar to the moment method, the set of variables is enlarged to contain non-equilibrium variables, our approach still uses the basic equilibrium variables and fulfills the main conditions of local thermodynamic equilibrium (classical thermal and caloric equations of state, Gibbs equation). However, the additional term in the entropy flux yields additional terms in the entropy generation, which, as will be seen, can still be written as a sum of products of forces and fluxes, but now the fluxes appear explicitly in the forces, i.e., the fluxes are coupled through the additional terms in the forces.

We shall show that the conservation laws together with the resulting coupled constitutive relations (CCR) can capture many interesting non-equilibrium effects, such as Knudsen paradox, transpiration flows, thermal stress, heat flux without temperature gradients, etc., in good agreement with experiments and with kinetic theory, e.g., the solution of the Boltzmann equation.

The remainder of the paper is structured as follows. The derivation of the CCR for the conservation laws is detailed in § 2. A thermodynamically consistent set of boundary conditions complementing the system of the conservation laws closed with the CCR (referred to as the *CCR system* hereafter) is presented in § 3. The linear stability of the CCR system is analyzed in § 4 to show that the CCR system is stable to small perturbations. Classical flow problems of Knudsen minimum and heat transfer in an isothermal lid-driven cavity are investigated in § 5. The paper ends with conclusions in § 6.

2 Derivation of coupled constitutive relations

The conservation laws, which are evolution equations for mass density ρ, macroscopic velocity v_i, and temperature T, read

$$\frac{\mathrm{D}\rho}{\mathrm{D}t} + \rho\frac{\partial v_k}{\partial x_k} = 0, \tag{1}$$

$$\rho\frac{\mathrm{D}v_i}{\mathrm{D}t} + \frac{\partial p}{\partial x_i} + \frac{\partial \Pi_{ik}}{\partial x_k} = \rho F_i, \tag{2}$$

$$\rho c_\mathrm{v}\frac{\mathrm{D}T}{\mathrm{D}t} + p\frac{\partial v_k}{\partial x_k} + \frac{\partial q_k}{\partial x_k} + \Pi_{kl}\frac{\partial v_k}{\partial x_l} = 0. \tag{3}$$

Here, $\frac{\mathrm{D}}{\mathrm{D}t}$ denotes the convective time derivative, p is the pressure, Π_{ik} is the viscous stress tensor, q_k is the heat flux and F_i is the external force per unit mass. Throughout the paper, Einstein summation is assumed over the repeated indices unless stated otherwise.

We shall consider monatomic ideal gases only, for which the pressure is $p = \rho \mathrm{R} T$ with R being the gas constant and specific internal energy is $u = c_\mathrm{v} T$ with the specific heat $c_\mathrm{v} = 3\mathrm{R}/2$. Moreover, for monatomic ideal gases the stress tensor is symmetric and tracefree, i.e., $\Pi_{kk} = 0$ [2].

It should be noted that conservation laws (1)–(3) contain the stress tensor Π_{ik} and heat flux q_k as unknowns, hence constitutive equations are required, which link the these quantities to the variables ρ, v_i and T.

The second law of thermodynamics states that the total entropy of an isolated system can never decrease over time [10, 13], that is

$$\rho\frac{\mathrm{D}s}{\mathrm{D}t} + \frac{\partial \Psi_k}{\partial x_k} = \Sigma \geq 0, \tag{4}$$

where s denotes the specific entropy, Ψ_k is the non-convective entropy flux and Σ is the non-negative entropy generation rate. An important aspect of a constitutive theory is to determine the appropriate relations among the properties s, Ψ_k, Σ and the variables ρ, v_i, T and their gradients so that the closed conservation laws guarantee the second law of thermodynamics.

2.1 Uncoupled constitutive relations: The NSF equations

In LIT, the constitutive relations for closing the system of conservation laws (1)–(3), are obtained such that the second law of thermodynamics is satisfied for all thermodynamic processes. For this, in LIT, local thermodynamic equilibrium is assumed [10, 12], which implies the local validity of the Gibbs equation

$$T\,\mathrm{d}s = \mathrm{d}u - \frac{p}{\rho^2}\,\mathrm{d}\rho. \tag{5}$$

For convenience, we shall write temperature T in energy units as $\theta = \mathrm{R}T$, and dimensionless entropy as $\eta = s/\mathrm{R}$, so that the Gibbs equation (5) for a monatomic ideal gas leads to

$$\frac{\mathrm{D}\eta}{\mathrm{D}t} = \frac{3}{2\theta}\frac{\mathrm{D}\theta}{\mathrm{D}t} - \frac{1}{\rho}\frac{\mathrm{D}\rho}{\mathrm{D}t}. \tag{6}$$

Multiplying eq. (6) with ρ, and replacing $\mathrm{D}\rho/\mathrm{D}t$, and $\mathrm{D}\theta/\mathrm{D}t$ using the mass balance equation (1) and the energy balance equation (3), one obtains the entropy balance equation for LIT,

$$\rho\frac{\mathrm{D}\eta}{\mathrm{D}t} + \frac{\partial}{\partial x_k}\left(\frac{q_k}{\theta}\right) = -\frac{\Pi_{kl}}{\theta}\frac{\partial v_k}{\partial x_l} - \frac{q_k}{\theta}\frac{\partial \ln\theta}{\partial x_k}. \tag{7}$$

Comparison of eq. (7) with eq. (4) gives the LIT expression for non-convective entropy flux as $\Psi_k = q_k/\theta$ and that for the entropy production term as

$$\Sigma = -\frac{1}{\theta}\left(\Pi_{kl}\frac{\partial v_{\langle k}}{\partial x_{l\rangle}} + \frac{q_k}{\theta}\frac{\partial\theta}{\partial x_k}\right). \tag{8}$$

The angular brackets around indices represent the symmetric and traceless part of a tensor, for example,

$$\frac{\partial v_{\langle i}}{\partial x_{j\rangle}} = \frac{1}{2}\left(\frac{\partial v_i}{\partial x_j} + \frac{\partial v_j}{\partial x_i}\right) - \frac{1}{3}\frac{\partial v_k}{\partial x_k}\delta_{ij}, \tag{9}$$

where δ_{ij} being the Kronecker delta tensor.

The entropy production (8) assumes a canonical form, i.e.,

$$\Sigma = \sum_\alpha \mathcal{J}_\alpha \mathcal{X}_\alpha,$$

with the thermodynamic fluxes, $\mathcal{J}_\alpha = \{\Pi_{kl}, q_k\}_\alpha$ and the thermodynamic forces $\mathcal{X}_\alpha = -\frac{1}{\theta}\left\{\frac{\partial v_{\langle k}}{\partial x_{l\rangle}}, \frac{1}{\theta}\frac{\partial\theta}{\partial x_k}\right\}_\alpha$. The phenomenological closure of LIT demands a linear relation between fluxes and forces of the form $\mathcal{J}_\alpha = \sum_\beta \mathcal{L}_{\alpha\beta}\mathcal{X}_\beta$, where he matrix of phenomenological coefficients depends only on equilibrium properties, $\mathcal{L}_{\alpha\beta}(\rho,\theta)$, and must be non-negative definite. For proper transformations between different observer frames, stress and heat flux must be Galilean invariant tensors [13], and it follows that only forces and fluxes of the same tensor type (scalars, vectors, 2-tensors, etc.) can be linked (Curie Principle [10]). Accordingly,

$$\Pi_{ij} = -2\mu\frac{\partial v_{\langle i}}{\partial x_{j\rangle}} \qquad \text{and} \qquad q_i = -\kappa\frac{\partial\theta}{\partial x_i}, \tag{10}$$

where μ and κ are the positive coefficients of shear viscosity and thermal conductivity, respectively, where factors with θ are absorbed in the coefficients.

It is worth pointing out that for a monatomic ideal gas interacting with power potentials, the viscosity depends on temperature alone as

$$\mu = \mu_0\left(\frac{\theta}{\theta_0}\right)^w, \tag{11}$$

where μ_0 is the viscosity at a reference temperature θ_0 and w is referred to as the viscosity exponent [2, 16]. Furthermore, the heat conductivity is proportional to viscosity, $\kappa = \frac{5\mu}{2\mathrm{Pr}}$, where $\mathrm{Pr} \simeq 2/3$ denotes the Prandtl number [2].

Relations $(10)_1$ and $(10)_2$ are the Navier–Stokes law and Fourier's law, respectively, and we refer to them as the linear *uncoupled constitutive relations*—emanating from LIT. When relations (10) are substituted in conservation laws (1)–(3), they yield the well-known compressible NSF equations of hydrodynamics.

2.2 Coupled constitutive relations

As mentioned in the introduction, LIT and RT yield identical results for simple fluids—such as ideal gases—but differ in their assumptions. Indeed, RT assumes the entropy flux $\Psi_k = q_k/\theta$ that is an outcome in LIT. In a recent paper [32], Paolucci & Paolucci considered entropy flux as function of the hydrodynamic variables and their gradients in a complete non-linear representation, but found that only the classical term $\Psi_k = q_k/\theta$ is compatible with the second law of thermodynamics. Nevertheless, allowing higher order contributions for stress and heat flux, they found additions which are fully non-linear in the gradients. Extended Irreversible Thermodynamics [15, 33] is similar to LIT, only that non-equilibrium variables, in particular stress and heat flux, are added, with additional contributions to the Gibbs equation, in an attempt to go beyond local thermodynamic equilibrium. RET [15] proceeds differently, but also adds non-equilibrium variables, and yields a non-equilibrium Gibbs equation. The consideration of local non-equilibrium gives additions to the LIT entropy flux, which appears as explicit function of the extended set of variables.

In theories of extended thermodynamics for 13 moments, stress tensor Π_{kl} and heat flux q_i are independent variables [15, 33], and the entropy flux is expressed through these. Using representation theorems for isotropic tensor functions [13] and dimensional analysis, we find the most general entropy flux expression for these variables as

$$\Psi_k = \gamma \frac{q_k}{\theta} - \alpha \frac{\Pi_{kl} q_l}{p\theta} + \beta \frac{\Pi_{kl}\Pi_{lm} q_m}{p^2\theta}, \tag{12}$$

where the dimensionless coefficients γ, α, β depend on the dimensionless invariants $\left(\Pi^2\right)_{ll}/p^2$, $\left(\Pi^3\right)_{ll}/p^3$, $q^2/(p^2\theta)$ (note that the invariant $\Pi_{kk} = 0$) [13].

Presently, we are only interested in the leading correction to the classical entropy flux q_i/θ. Considering Π_{ij} and q_i as small and of the same order, Taylor expansion to second order yields

$$\Psi_k = \frac{q_k}{\theta} - \alpha_0 \frac{\Pi_{kl} q_l}{p\theta}, \tag{13}$$

where the coefficient of the first term on the right-hand side was chosen such that the classical result is reproduced, and α_0 is a constant. The form (13) of the entropy flux appears as a result in RET of 13 moments (with $\alpha_0 = 2/5$) [15].

Interestingly, the gradient of the additional term $\alpha_0 \frac{\Pi_{kl} q_l}{p\theta}$ can be expanded such that it yields higher order additions to the thermodynamic forces. Indeed, introduction of this additional contribution in eq. (7), yields an extended form of the second law that reads

$$\begin{aligned}
&\rho \frac{\mathrm{D}\eta}{\mathrm{D}t} + \frac{\partial}{\partial x_k}\left(\frac{q_k}{\theta} - \underline{\alpha_0 \frac{\Pi_{kl} q_l}{p\theta}}\right) \\
&\qquad = -\frac{\Pi_{kl}}{\theta}\left[\frac{\partial v_{\langle k}}{\partial x_{l\rangle}} + \underline{\frac{\alpha_0}{p}\left(\frac{\partial q_{\langle l}}{\partial x_{k\rangle}} - \alpha_1 q_{\langle k}\frac{\partial \ln\theta}{\partial x_{l\rangle}} - \alpha_2 q_{\langle k}\frac{\partial \ln p}{\partial x_{l\rangle}}\right)}\right] \\
&\qquad\qquad - \frac{q_k}{\theta^2}\left[\frac{\partial\theta}{\partial x_k} + \underline{\frac{\alpha_0}{\rho}\left(\frac{\partial \Pi_{kl}}{\partial x_l} - \alpha_1^* \Pi_{kl}\frac{\partial \ln\theta}{\partial x_l} - \alpha_2^* \Pi_{kl}\frac{\partial \ln p}{\partial x_l}\right)}\right].
\end{aligned} \tag{14}$$

The underlined terms on the left are equal to the underlined terms on the right, where α_1 and α_2 are arbitrary numbers, and $\alpha_r^* = 1 - \alpha_r$, $r \in \{1, 2\}$. The coefficients α_r and α_r^* distribute the contributions to entropy generation between different force-flux pairs; their values will be obtained from comparison to results from kinetic theory. For $\alpha_0 = 0$, the underlined terms in eq. (14) vanish, and eq. (7) is recovered.

The right-hand side of eq. (14) is the entropy generation rate, which can—again—be recognized as a sum of products of the fluxes Π_{kl} and q_k with generalized thermodynamic forces (in square brackets). The corresponding phenomenological equations that guarantee positivity of the entropy production read

$$\Pi_{kl} = -2\mu \left[\frac{\partial v_{\langle l}}{\partial x_{k\rangle}} + \frac{\alpha_0}{p} \left(\frac{\partial q_{\langle l}}{\partial x_{k\rangle}} - \alpha_1 q_{\langle k} \frac{\partial \ln \theta}{\partial x_{l\rangle}} - \alpha_2 q_{\langle k} \frac{\partial \ln p}{\partial x_{l\rangle}} \right) \right] \tag{15}$$

and

$$q_k = -\frac{5\mu}{2\,\mathrm{Pr}} \left[\frac{\partial \theta}{\partial x_k} + \frac{\alpha_0}{\rho} \left(\frac{\partial \Pi_{kl}}{\partial x_l} - \alpha_1^* \Pi_{kl} \frac{\partial \ln \theta}{\partial x_l} - \alpha_2^* \Pi_{kl} \frac{\partial \ln p}{\partial x_l} \right) \right]. \tag{16}$$

Here, the coefficients were chosen such that in the classical limit (i.e., when $\alpha_0 = 0$), the NSF equations are obtained. Since the fluxes Π_{kl} and q_k appear explicitly in the forces, we refer to relations (15) and (16) as the coupled constitutive relations (CCR) for conservation laws (1)–(3). Conservation laws (1)–(3) along with CCR (15) and (16) constitute the *CCR system*.

We emphasize that only the entropy flux was changed, while the Gibbs equation, and hence entropy, remain unchanged. With their higher order contributions to the fluxes and the equilibrium entropy, the resulting equations stand somewhere between the NSF equations and higher order models such as the Burnett equations. Since the CCR system is accompanied by the second law, we expect it to be stable while, as pointed out before, the Burnett equations are not accompanied by a proper entropy balance, and are unstable.

With the extended entropy flux (13) and coupling force-flux relations, we find additional linear contributions to stress and heat flux, in contrast to [32] where all additional contributions are strictly non-linear. The linear contributions are well known in kinetic theory, and are required to describe processes. For instance, the linear contribution $\frac{\partial q_{\langle l}}{\partial x_{k\rangle}}$ in (15) describes thermal stresses, where temperature gradients can induce flow [4]. Similarly, the linear contribution $\frac{\partial \Pi_{kl}}{\partial x_l}$ in (16) describes stress induced heat flux, as discussed in § 5(b) below.

2.3 Evaluation of the phenomenological coefficients

The CCR (15) and (16) contain the coefficients α_0, α_1 and α_2, which, in principle, can be determined from experiments or theoretical scenarios. While the Burnett equations are unstable in transient processes, they describe higher order effects in gases with some accuracy. Hence, we determine the CCR coefficients from comparison with the Burnett equations.

The Burnett equations are obtained from the CE expansion in the Knudsen number, which is proportional to the viscosity. The procedure can be easily applied to the constitutive relations (15) and (16) as follows: Stress and heat flux are expanded in terms of the viscosity, so that

$$\left.\begin{aligned} \Pi_{kl} &= \mu \Pi_{kl}^{(1)} + \mu^2 \Pi_{kl}^{(2)} + \cdots \\ q_k &= \mu q_k^{(1)} + \mu^2 q_k^{(2)} + \cdots \end{aligned}\right\} \tag{17}$$

Inserting this ansatz into eqs. (15) and (16), we find at first order the NSF laws

$$\Pi_{kl}^{(1)} = -2 \frac{\partial v_{\langle k}}{\partial x_{l\rangle}} = -2 S_{kl} \qquad \text{and} \qquad q_k^{(1)} = -\frac{5}{2\,\mathrm{Pr}} \frac{\partial \theta}{\partial x_k}, \tag{18}$$

and at second order

$$\Pi_{kl}^{(2)} = \frac{5\alpha_0}{\mathrm{Pr}}\frac{1}{p}\left[\frac{\partial^2\theta}{\partial x_{\langle k}\partial x_{l\rangle}} - \alpha_2\frac{\partial\theta}{\partial x_{\langle k}}\frac{\partial \ln p}{\partial x_{l\rangle}} + (w-\alpha_1)\frac{\partial\theta}{\partial x_{\langle k}}\frac{\partial \ln\theta}{\partial x_{l\rangle}}\right], \tag{19}$$

$$q_k^{(2)} = \frac{5\alpha_0}{\mathrm{Pr}}\frac{1}{\rho}\left[\frac{\partial S_{kl}}{\partial x_l} - \alpha_2^* S_{kl}\frac{\partial \ln p}{\partial x_l} + \left(w - \alpha_1^* + \frac{1}{\alpha_0}\right) S_{kl}\frac{\partial \ln\theta}{\partial x_l}\right], \tag{20}$$

where w is the exponent in the expression of viscosity for power potentials, see eq. (11). Comparison of (19) and (20) with the Burnett constitutive relations [eqs. (4.47) and (4.48) of [2], respectively] gives

$$\left.\begin{aligned} \alpha_0 &= \frac{\mathrm{Pr}}{5}\varpi_3, & -\frac{5\alpha_0}{\mathrm{Pr}}\alpha_2 &= \varpi_4, & \frac{5\alpha_0}{\mathrm{Pr}}(w-\alpha_1) &= \varpi_5,\\ \alpha_0 &= \frac{\mathrm{Pr}}{5}\theta_4, & -\frac{5\alpha_0}{\mathrm{Pr}}(1-\alpha_2) &= \theta_3, & \frac{5\alpha_0}{\mathrm{Pr}}\left(w-1+\alpha_1+\frac{1}{\alpha_0}\right) &= 3\theta_5, \end{aligned}\right\} \tag{21}$$

where, ϖ_i and θ_i are the Burnett coefficients. These relations (21) yield the unknown coefficients as

$$\alpha_0 = \frac{\mathrm{Pr}}{5}\varpi_3, \qquad \alpha_2 = -\frac{\varpi_4}{\varpi_3}, \qquad \alpha_1 = w - \frac{\varpi_5}{\varpi_3} \quad \text{or} \quad \alpha_1 = 1 - w + 3\frac{\theta_5}{\varpi_3} - \frac{5}{\mathrm{Pr}}\frac{1}{\varpi_3}.$$

We note that the CCR coefficients α_0, α_1, α_2 can be fitted to the Burnett coefficients in agreement with the well-known relations between Burnett coefficients, $\theta_4 = \varpi_3$ and $\varpi_3 + \varpi_4 + \theta_3 = 0$ [2, 34].

The Burnett coefficients depend upon the choice of intermolecular potential function appearing in the Boltzmann collision operator, values of these coefficients for inverse-power law potentials can be found, for example, in Ref. [2, 35]. The values of the phenomenological coefficients α_0, α_1 and α_2 for the hard-sphere (HS) and Maxwell molecule (MM) gases are given in table 1; for other power potentials, they can be computed from eqs. (21). We emphasize that

Table 1: Phenomenological coefficients for hard sphere (HS) and Maxwell molecule (MM) gases

Molecule type	Pr	α_0	α_2	α_1
MM	2/3	2/5	0	0
HS	0.661	0.3197	−0.2816	0.4094

we have performed the expansion (17) only to determine the coefficients α_0, α_1, α_2, but will use the full CCR as given in (15) and (16).

3 Wall boundary conditions

Just as the process of finding constitutive relations in the bulk, the development of wall boundary conditions is based on the second law. Specifically, one determines the entropy generation at the interface, and finds the boundary conditions as phenomenological laws that guarantee positivity of the entropy generation.

The entropy production rate at the boundary Σ_w is given by the difference between the entropy fluxes into and out of the surface [10], i.e.,

$$\Sigma_w = \left(\Psi_k - \frac{q_k^w}{\theta^w}\right) n_k \geq 0. \tag{22}$$

Here, n_k is unit normal pointing from the boundary into the gas , q_k^w denotes the heat flux in the wall at the interface, and θ^w denotes the temperature of the wall at the interface. Here, the wall is assumed to be a rigid Fourier heat conductor, with the entropy flux q_k^w/θ^w and $\Pi_{ik}^w = 0$.

At the the interface, the total fluxes of mass, momentum and energy are continuous, due to conservation of these quantities [10, 31, 36, 37],

$$\left.\begin{aligned} v_k n_k = v_k^w n_k = 0, \\ \big(p\delta_{ik} + \Pi_{ik}\big) n_k = p^w n_i, \\ \big(p v_k + \Pi_{ik} v_i + q_k\big) n_k = \big(p^w v_k^w + q_k^w\big) n_k, \end{aligned}\right\} \tag{23}$$

where all quantities with superscript w refer to wall properties, and the others refer to the gas properties. To proceed, we combine entropy generation and continuity conditions by eliminating the heat flux in the wall q_k^w, and the pressure p^w, and find, after insertion of the entropy flux (13),

$$\Sigma_w = -\left[\frac{q_k}{\theta\theta^w}\mathcal{T} + \Pi_{ik}\left(\alpha_0\frac{q_i}{p\theta} + \frac{\mathcal{V}_i}{\theta^w}\right)\right] n_k \geq 0. \tag{24}$$

Here, $\mathcal{V}_i = v_i - v_i^w$ is the slip velocity, with $\mathcal{V}_i n_i = 0$, and $\mathcal{T} = \theta - \theta^w$ is the temperature jump.

To write the entropy generation properly as sum of products of forces and fluxes, it is necessary to decompose the stress tensor and heat flux into their components in the normal and tangential directions as [31]

$$\Pi_{ij} = \Pi_{nn}\left(\frac{3}{2}n_i n_j - \frac{1}{2}\delta_{ij}\right) + \bar{\Pi}_{ni} n_j + \bar{\Pi}_{nj} n_i + \widetilde{\Pi}_{ij}, \quad \text{and} \quad q_i = q_n n_i + \bar{q}_i, \tag{25}$$

where $q_n = q_k n_k$, $\Pi_{nn} = \Pi_{kl} n_k n_l$, and

$$\left.\begin{aligned} \bar{q}_i &= q_i - q_n n_i, \\ \bar{\Pi}_{ni} &= \Pi_{ik} n_k - \Pi_{nn} n_i, \\ \widetilde{\Pi}_{ij} &= \Pi_{ij} - \Pi_{nn}\left(\frac{3}{2}n_i n_j - \frac{1}{2}\delta_{ij}\right) - \bar{\Pi}_{ni} n_j - \bar{\Pi}_{nj} n_i, \end{aligned}\right\} \tag{26}$$

such that $\bar{q}_k n_k = \bar{\Pi}_{nk} n_k = \widetilde{\Pi}_{kk} = \widetilde{\Pi}_{ij} n_j = \widetilde{\Pi}_{ij} n_i = 0$, see appendix A for more details.

Substituting eqs. (25) and (26) into eq. (24), the entropy generation can be written as a sum of two contributions,

$$\Sigma_w = -\frac{\bar{\Pi}_{ni}}{p\,\theta}\big(\mathcal{P}\mathcal{V}_i + \alpha_0\bar{q}_i\big) - \frac{(q_n + \bar{\Pi}_{ni}\mathcal{V}_i)}{p\,\theta\theta^w}\big(\mathcal{P}\mathcal{T} + \alpha_0\Pi_{nn}\theta\big).$$

where $\mathcal{P} = p - \alpha_0\Pi_{nn}$. As in LIT of the bulk, the positivity of entropy production is ensured by phenomenological equations,

$$\bar{\Pi}_{ni} = -\frac{\varsigma_1}{\sqrt{\theta}}\big(\mathcal{P}\mathcal{V}_i + \alpha_0\bar{q}_i\big) \qquad \text{and} \qquad q_n + \bar{\Pi}_{ni}\mathcal{V}_i = -\frac{\varsigma_2}{\sqrt{\theta}}\big(\mathcal{P}\mathcal{T} + \alpha_0\Pi_{nn}\theta\big). \tag{27}$$

Here, ς_1 and ς_2 are non-negative coefficients, which can be obtained either from experiments or from kinetic theory models. We determine ς_1 and ς_2 from the Maxwell accommodation model [38]. This model employs the accommodation coefficient χ, which is defined such that a fraction χ of the molecules hitting the wall returns to the gas in equilibrium with the wall properties (wall Maxwellian), whereas the remaining fraction $(1-\chi)$ is specularly reflected. Comparison with boundary conditions from this model shows that these coefficients are related to the velocity-slip coefficient η_{VS} and the temperature-jump coefficient η_{TJ} as [31]

$$\varsigma_1 = \sqrt{\frac{2}{\pi}}\frac{\chi}{2-\chi}\frac{1}{\eta_{\mathrm{VS}}}, \quad \text{and} \quad \varsigma_2 = \sqrt{\frac{2}{\pi}}\frac{\chi}{2-\chi}\frac{2}{\eta_{\mathrm{TJ}}}. \tag{28}$$

The values of velocity-slip coefficient η_{VS} and the temperature-jump coefficient η_{TJ} as obtained from the linearized Boltzmann equation [39–42] are given in table 2.

Table 2: Velocity-slip coefficient $\eta_{\rm VS}$ and the temperature-jump coefficient $\eta_{\rm TJ}$ for hard sphere (HS) and Maxwell molecule (MM) gases obtained through the linearized Boltzmann equation in Refs. [39–42]

Molecule type	$\eta_{\rm VS}$	$\eta_{\rm TJ}$
MM	1.1366 [39]	1.1621 [41]
HS	1.1141 [40]	1.1267 [42]

Conditions (27) are the required, and thermodynamically consistent, boundary conditions for the CCR system. The first term in the brackets of boundary condition $(27)_1$ relates the shear stress ($\bar{\Pi}_{ni}$) to the tangential velocity slip ($\mathcal{V}_i$) while the second term describes thermal transpiration—a flow induced by the tangential heat flux. It is evident from the boundary condition $(27)_1$ that the NSF equations, for which $\alpha_0 = 0$, do not allow thermal transpiration within the framework of thermodynamically consistent boundary conditions. The boundary condition $(27)_2$ relates temperature jump ($\mathcal{T}$) and viscous heating ($\bar{\Pi}_{ni}\mathcal{V}_i$) to the normal heat flux q_n (see [43]).

Several authors have suggested second order boundary conditions for the Navier–Stokes equations, which are in a form, possibly with other values of coefficients, identical to (27) [44]. Our derivation suggests that in order for the boundary conditions to be compatible with the second law of thermodynamics, the NSF equations do not suffice, while they arise quite naturally from CCR.

4 Linear stability analysis

In this section, we analyze the stability of the CCR system ((1)–(3) along with (15) and (16)) to small perturbations.

4.1 Linear dimensionless equations

For linear stability analysis, the CCR system is linearized by introducing small perturbations in the field variables from their values in an equilibrium rest state. We write

$$\rho = \rho_0(1+\hat{\rho}), \quad v_i = \sqrt{\theta_0}\,\hat{v}_i, \quad \theta = \theta_0(1+\hat{\theta}), \quad \Pi_{ij} = \rho_0\theta_0\hat{\Pi}_{ij}, \quad q_i = \rho_0\theta_0\sqrt{\theta_0}\,\hat{q}_i, \tag{29}$$

where ρ_0 and θ_0 are the values of ρ and θ in the equilibrium while the remaining variables vanish in the equilibrium rest state; hats denote the dimensionless perturbations in the field variables from their values in the equilibrium rest state; and $\sqrt{\theta_0}$ is the scale for making the velocity dimensionless. These dimensionless perturbations are assumed to be much smaller than unity so that the linear analysis remains valid. Consequently, the pressure is linearized as $p = p_0(1+\hat{p})$ with $p_0 = \rho_0\theta_0$ and $\hat{p} \approx \hat{\rho}+\hat{\theta}$. Furthermore, a relevant length scale L is introduced so that the dimensionless space variable is $\hat{x}_i = x_i/L$ and the dimensionless time is $\hat{t} = t\sqrt{\theta_0}/L$. Also, the external force is assumed to be small (of the order of small perturbations) in a linear analysis, and the dimensionless external force is given by $\hat{F}_i = F_iL/\theta_0$. Substituting the values of field variables from eqs. (29) in the CCR system, introducing the dimensionless space and time variables, and retaining only the linear terms in the perturbation variables, one obtains

$$\frac{\partial\rho}{\partial t} + \frac{\partial v_k}{\partial x_k} = 0, \tag{30}$$

$$\frac{\partial v_i}{\partial t} + \frac{\partial p}{\partial x_i} + \frac{\partial\Pi_{ik}}{\partial x_k} = F_i, \tag{31}$$

$$\frac{3}{2}\frac{\partial\theta}{\partial t} + \frac{\partial v_k}{\partial x_k} + \frac{\partial q_k}{\partial x_k} = 0 \tag{32}$$

with

$$\Pi_{kl} = -2\mathrm{Kn}\left(\frac{\partial v_{\langle l}}{\partial x_{k\rangle}} + \alpha_0 \frac{\partial q_{\langle l}}{\partial x_{k\rangle}}\right) \quad \text{and} \quad q_k = -\frac{5}{2}\frac{\mathrm{Kn}}{\mathrm{Pr}}\left(\frac{\partial \theta}{\partial x_k} + \alpha_0 \frac{\partial \Pi_{kl}}{\partial x_l}\right). \tag{33}$$

In eqs. (30)–(33), the hats are dropped for better readability, and

$$\mathrm{Kn} = \frac{\mu_0}{\rho_0 \sqrt{\theta_0} L} \tag{34}$$

is the Knudsen number with μ_0 being the viscosity of the gas in equilibrium. Thus, all quantities in eqs. (30)–(33) and henceforth are dimensionless unless otherwise mentioned.

4.2 Plane harmonic waves

Now we consider a one-dimensional process (in the x-direction) without any external forces (i.e., $F_i = 0$) and assume a plane wave solution of the form

$$\boldsymbol{\psi} = \mathring{\boldsymbol{\psi}} \exp\left[\mathbb{i}(\omega t - kx)\right] \tag{35}$$

for eqs. (30)–(33), where $\boldsymbol{\psi} = \{\rho, v_x, \theta, \Pi_{xx}, q_x\}^\top$, $\mathring{\boldsymbol{\psi}}$ is a vector containing the complex amplitudes of the respective waves, ω is the (dimensionless) frequency and k is the (dimensionless) wavenumber. Substitution of the plane wave solution (35) into eqs. (30)–(33) gives a system of algebraic equations $\mathcal{A}\boldsymbol{\psi} = \mathbf{0}$, where

$$\mathcal{A} = \begin{bmatrix} \mathbb{i}\omega & -\mathbb{i}k & 0 & 0 & 0 \\ -\mathbb{i}k & \mathbb{i}\omega & -\mathbb{i}k & -\mathbb{i}k & 0 \\ 0 & -\mathbb{i}k & \frac{3}{2}\mathbb{i}\omega & 0 & -\mathbb{i}k \\ 0 & -\frac{4}{3}\mathrm{Kn}\,\mathbb{i}k & 0 & 1 & -\frac{4}{3}\mathrm{Kn}\,\alpha_0 \mathbb{i}k \\ 0 & 0 & -\frac{5}{2}\frac{\mathrm{Kn}}{\mathrm{Pr}}\mathbb{i}k & -\frac{5}{2}\frac{\mathrm{Kn}}{\mathrm{Pr}}\alpha_0 \mathbb{i}k & 1 \end{bmatrix}.$$

For nontrivial solutions, the determinant of matrix $\mathcal{A}$ must vanish, i.e., $\det(\mathcal{A}) = 0$. This leads to the dispersion relation, which is the relation between ω and k:

$$\left(\frac{3}{2} + 5\frac{\mathrm{Kn}^2}{\mathrm{Pr}}\alpha_0^2 k^2\right)\omega^3 - \mathbb{i}\left(2\mathrm{Kn} + \frac{5}{2}\frac{\mathrm{Kn}}{\mathrm{Pr}}\right)k^2\omega^2 - \frac{5}{2}\left[1 + \frac{2}{3}\frac{\mathrm{Kn}^2}{\mathrm{Pr}}(2 - 4\alpha_0 + 5\alpha_0^2)k^2\right]k^2\omega + \frac{5}{2}\frac{\mathrm{Kn}}{\mathrm{Pr}}\mathbb{i}\,k^4 = 0. \tag{36}$$

For temporal stability, a disturbance is considered in space; consequently, the wavenumber k is assumed to be real while the frequency ω can be complex. From the plane wave solution (35), it is clear that temporal stability requires the imaginary part of the frequency to be nonnegative, i.e., $\mathrm{Im}(\omega) \geq 0$, for all wavenumbers. In other words, if $\mathrm{Im}(\omega) < 0$, then a small disturbance in space will blow up in time.

Figure 1 illustrates the stability diagram for the CCR system, NSF equations and Burnett equations shown by blue, red and green colors, respectively. The results for the NSF equations and Burnett equations are included for comparison. Assuming Maxwell molecules, we have $\mathrm{Pr} = 2/3$ and $\alpha_0 = 2/5$; the Knudsen number is set to $\mathrm{Kn} = 1$, that is the mean free path is used as relevant length scale. The figure exhibits $\omega(k) = \mathrm{Re}(\omega) + \mathbb{i}\,\mathrm{Im}(\omega)$—obtained from the dispersion relations for the CCR system, NSF equations and Burnett equations—in the complex plane with k as parameter. The gray region in the figure is the region, in which the stability conditions are not fulfilled, hence it depicts the unstable region whereas the white region represents the stable one.

It is evident from figure 1 that the NSF equations (red) as well as the CCR system (blue) are linearly stable in time for all wavenumbers since the roots of their dispersion relations always have nonnegative imaginary parts; on the other hand, the Burnett equations (green) are unstable in time, with negative roots for large wavenumbers.

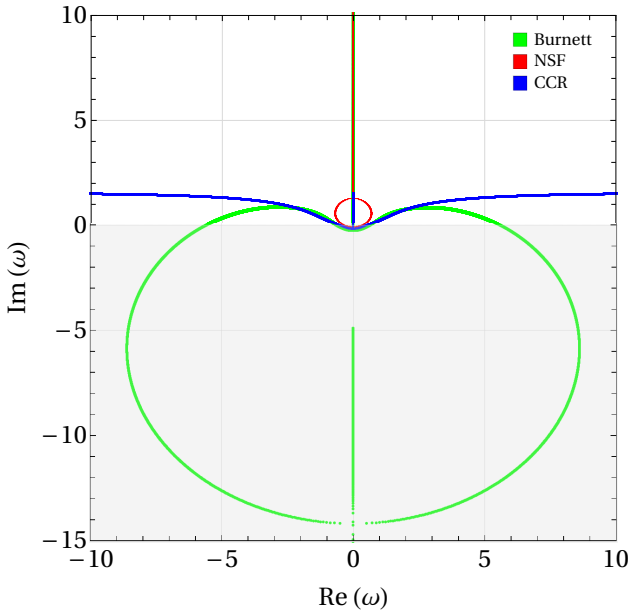

Figure 1: Temporal stability diagram for the CCR system (blue), NSF equations (red) and Burnett equations (green). The roots ω of the dispersion relations plotted in the complex plane for different values of k. The gray and white colors depict the unstable and stable regions, respectively.

5 Classical flow problems

5.1 Knudsen minimum

The Knudsen minimum is observed in a force-driven Poiseuille flow of rarefied gases, in which, for given force, the mass flow rate of a gas first decreases with the Knudsen number, attains a minimum value around a critical Knudsen number and then increases with the Knudsen number. We shall investigate this problem through the CCR system.

Let us consider the steady state ($\partial(\cdot)/\partial t = 0$) of a gas confined between two isothermal, fully diffusive walls of a channel. Let the walls be located at (dimensionless positions) $y = \mp 1/2$ and be kept at a (dimensionless) temperature $\theta^w = 1$. The flow is assumed to be fully developed and driven by a uniform (dimensionless) external force F in the positive x-direction parallel to the walls; all field variables are independent of x; and the velocity component in the y-direction is zero, i.e., $v_y = 0$. The problem can be described through the (linear-dimensionless) CCR system (eqs. (30)–(33)). For the problem under consideration, the mass balance equation (30) is identically satisfied and the rest of the equations simplify to

$$\frac{\partial \Pi_{xy}}{\partial y} = F, \qquad \frac{\partial \rho}{\partial y} + \frac{\partial \theta}{\partial y} + \frac{\partial \Pi_{yy}}{\partial y} = 0, \qquad \frac{\partial q_y}{\partial y} = 0 \tag{37}$$

with

$$\left.\begin{aligned} \Pi_{xy} &= -\mathrm{Kn}\left(\frac{\partial v_x}{\partial y} + \alpha_0 \frac{\partial q_x}{\partial y}\right), & \Pi_{yy} &= -\frac{4}{3}\mathrm{Kn}\,\alpha_0 \frac{\partial q_y}{\partial y}, \\ q_x &= -\frac{5}{2}\frac{\mathrm{Kn}}{\mathrm{Pr}}\alpha_0 \frac{\partial \Pi_{xy}}{\partial y}, & q_y &= -\frac{5}{2}\frac{\mathrm{Kn}}{\mathrm{Pr}}\left(\frac{\partial \theta}{\partial y} + \alpha_0 \frac{\partial \Pi_{yy}}{\partial y}\right). \end{aligned}\right\} \tag{38}$$

The boundary conditions (27) at the walls (i.e., at $y = \mp 1/2$) in the linear-dimensionless form reduce to

$$\pm \Pi_{xy} = -\varsigma_1 \left(v_x + \alpha_0\, q_x\right) \qquad \text{and} \qquad \pm\, q_y = -\varsigma_2\, \alpha_0\, \Pi_{yy}. \tag{39}$$

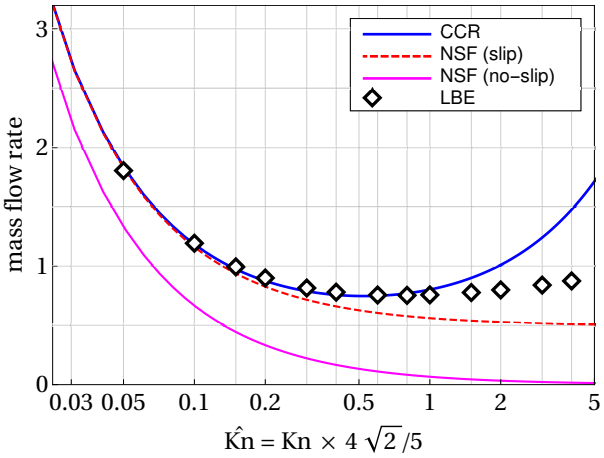

Figure 2: Mass flow rate of a hard-sphere gas in a force-driven Poiseuille flow plotted over the Knudsen number for $F = 1$. The accommodation coefficient is $\chi = 1$.

Solving equations $(37)_1$ and $(38)_{1,3}$ with boundary conditions $(39)_1$ yields a parabolic velocity profile,

$$v_x = -\frac{1}{2}\frac{1}{\mathrm{Kn}}F\left(y^2 - \frac{1}{4} - \frac{\mathrm{Kn}}{\varsigma_1} - 5\frac{\mathrm{Kn}^2}{\mathrm{Pr}}\alpha_0^2\right).$$

Consequently, the mass flow rate of the gas is

$$\frac{1}{\sqrt{2}}\int_{-1/2}^{1/2} v_x \,\mathrm{d}y = \frac{1}{2\sqrt{2}}F\left(\frac{1}{6}\frac{1}{\mathrm{Kn}} + \frac{1}{\varsigma_1} + 5\frac{\mathrm{Kn}}{\mathrm{Pr}}\alpha_0^2\right). \tag{40}$$

Here, the additional factor of $1/\sqrt{2}$ in the mass flow rate is included in order to compare the present results with those obtained from the linearized Boltzmann equation (LBE) in [5] where the authors scale velocity by $\sqrt{2\theta}$. As the walls of the channel are fully diffusive, the accommodation coefficient χ is unity, and hence from eq. $(28)_1$, $\varsigma_1 = (\sqrt{2/\pi})/\eta_{\mathrm{VS}}$. The mass flow rate from the NSF equations with slip boundary conditions is obtained by setting $\alpha_0 = 0$, which gives $\frac{1}{2\sqrt{2}}F\left(\frac{1}{6}\frac{1}{\mathrm{Kn}} + \frac{1}{\varsigma_1}\right)$, while for NSF with no-slip boundary conditions one finds $\frac{1}{12\sqrt{2}}\frac{1}{\mathrm{Kn}}F$.

Figure 2 shows the mass flow rate of a hard-sphere gas plotted over the Knudsen number $\hat{\mathrm{Kn}} = 4\sqrt{2}\,\mathrm{Kn}/5$ for $F = 1$, as obtained from the CCR system (blue solid line), from the NSF equations with (red dashed line) and without (magenta solid line) slip boundary conditions, and from the LBE (symbols). Again, the Knudsen number Kn is multiplied with a factor of $4\sqrt{2}/5$ in order to compare the results with those from [5]. The parameters Pr and η_{VS} for hard-spheres are taken from tables 1 and 2, respectively. It is clear from the figure that the CCR system predicts the Knudsen minimum and closely follow the mass flow rate profile from the LBE up to $\mathrm{Kn} \simeq 1$. On the other hand, the NSF equations with or without slip do not predict the Knudsen minimum at all; in particular, the mass flow rate from the NSF equations with no-slip boundary conditions is not even close to that from the LBE equations. The mass flow rate from the CCR system (eq. (40)) possesses the term $5\frac{\mathrm{Kn}}{\mathrm{Pr}}\alpha_0^2$, which dominates for large Knudsen numbers resulting into an increasing mass flow rate profile for large Knudsen numbers. However, such a term is not present in the expressions of mass flow rates obtained with the NSF equations with or without slip; consequently, the mass flow rate profiles from the NSF equations always decay with the Knudsen number.

5.2 Lid-driven cavity flow

The lid-driven cavity is a well-known test problem in rarefied gas dynamics, in which a gas—under no external force—is confined to a square enclosure of (dimensionless) length 1. The

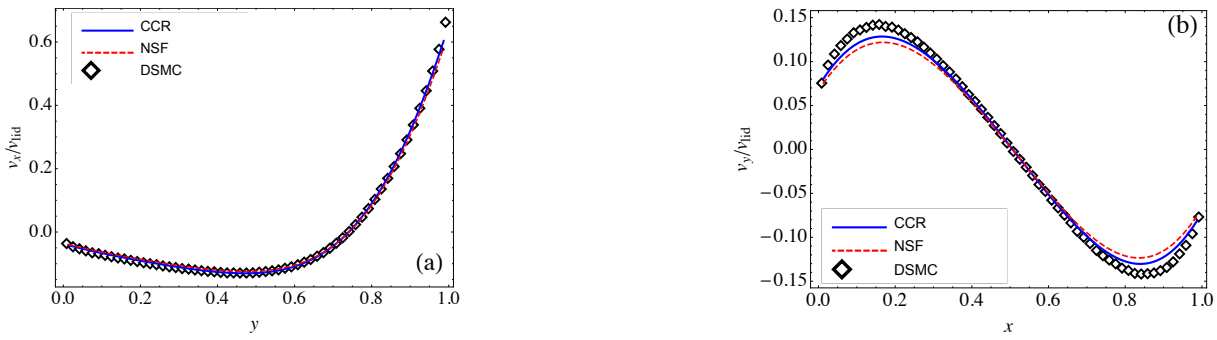

Figure 3: Dimensionless velocity profiles: (a) x-component of the velocity ($v_x/v_{\rm lid}$) along the vertical centerline of the cavity, and (b) y-component of the velocity ($v_y/v_{\rm lid}$) along the horizontal centerline of the cavity. Numerical solutions from the the CCR system (blue solid lines) and from the NSF equations (red dashed lines) for $\mathrm{Kn} = 0.1/\sqrt{2}$ are compared to the DSMC data (symbols) from [8].

boundaries at $x = 0$, $x = 1$ and $y = 0$ are stationary while the upper boundary at $y = 1$ is moving in the x-direction with a velocity $v_{\rm lid}$. The boundaries are kept at a constant temperature, which is equal to the initial temperature of the gas inside the cavity so that the dimensionless temperature of the walls $\theta^w = 1$. The flow in the cavity is assumed to be in steady state and independent of the z-direction, i.e., $\partial(\cdot)/\partial t = 0$ and $\partial(\cdot)/\partial z = 0$. The problem is solved through the CCR system ((1)–(3) along with (15) and (16) in dimensionless form) numerically using a finite difference scheme whose details can be found in [9].

Figure 3 shows the vertical and horizontal components of the velocity along the horizontal and vertical centerlines of the cavity, respectively, computed through the CCR system and the NSF equations for $\mathrm{Kn} = 0.1/\sqrt{2}$ and $v_{\rm lid} = 0.21$ (50 m/s in dimensional units). The results are compared to DSMC simulations for hard spheres, hence we chose the phenomenological coefficients for hard spheres from table 1. The velocity profiles from the CCR system as well as from the NSF equations are in good agreement with the DSMC simulations [8].

It is well-known that the classical NSF laws cannot describe heat transfer phenomena in a lid-driven cavity, see e.g., [9, 45, 46] and references therein. Therefore, either extended models, such as Grad-type moment equations or the R13 equations [2, 17], or other advanced constitutive laws ought to be used for the closure in order to describe the heat transfer characteristics.

We study in particular the temperature field and heat flux induced in the lid-driven cavity and compare the results from the CCR system to those from DSMC presented in [8]. Figure 4 illustrates the heat flux lines plotted over the temperature contours, and compares the predictions of (from left to right) the CCR system, DSMC and the NSF equations. The NSF equations predict that the heat flows from hot (top-right corner) to cold (top-left corner) in an orthogonal direction to the temperature contours. However, both the CCR system and DSMC predict heat flux from cold region to hot region, which is non-Fourier effect.

The non-Fourier heat flux can easily be understood from the linear terms itself, which dominate the nonlinear terms. From the (linearized) momentum balance equation (31) (ignoring the time derivative and external force terms), the divergence of the stress is given by

$$\frac{\partial \Pi_{ik}}{\partial x_k} = -\frac{\partial p}{\partial x_i}. \tag{41}$$

Substitution of this in the (linearized) constitutive relation for the heat flux $(33)_2$ yields

$$q_i \simeq Q_i = -\frac{5}{2}\frac{\mathrm{Kn}}{\mathrm{Pr}}\frac{\partial \theta}{\partial x_i} + \frac{5}{2}\frac{\mathrm{Kn}}{\mathrm{Pr}}\alpha_0\frac{\partial p}{\partial x_i}. \tag{42}$$

The first term on the right-hand side of eq. (42) is the Fourier's contribution to the heat flux while the second term is the non-Fourier contribution to the heat flux due to the pressure gradient,

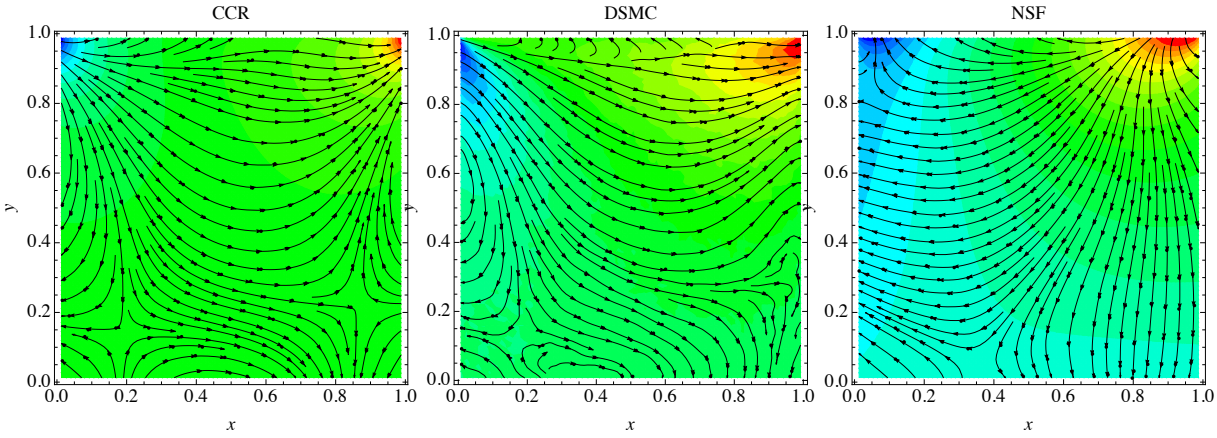

Figure 4: Heat flux lines superimposed over temperature contours for the lid-driven cavity problem at Kn $= 0.1/\sqrt{2}$ obtained through the CCR system (left) and the NSF equations (right) are compared to DSMC data (middle) given in [8].

which is responsible for heat transfer from the cold region to the hot one. Figure 5 displays heat flux lines (black) and Q_i lines (red) superimposed on the contours of $(\theta - \alpha_0 p)$ for the CCR system (left) and DSMC (right). It is evident from the figure that the heat flux q_i from (16) is estimated well with Q_i (eq. (42)), which is orthogonal to $(\theta - \alpha_0 p)$ contour lines. It can also be seen by comparing figures 4 and 5 that the heat flux lines in DSMC simulations are governed by the $(\theta - \alpha_0 p)$ gradients, not by the temperature alone. Near the bottom of the cavity, the heat flux lines (black) given by DSMC differ from those given by Q_i due to statistical noise inherent to the DSMC method.

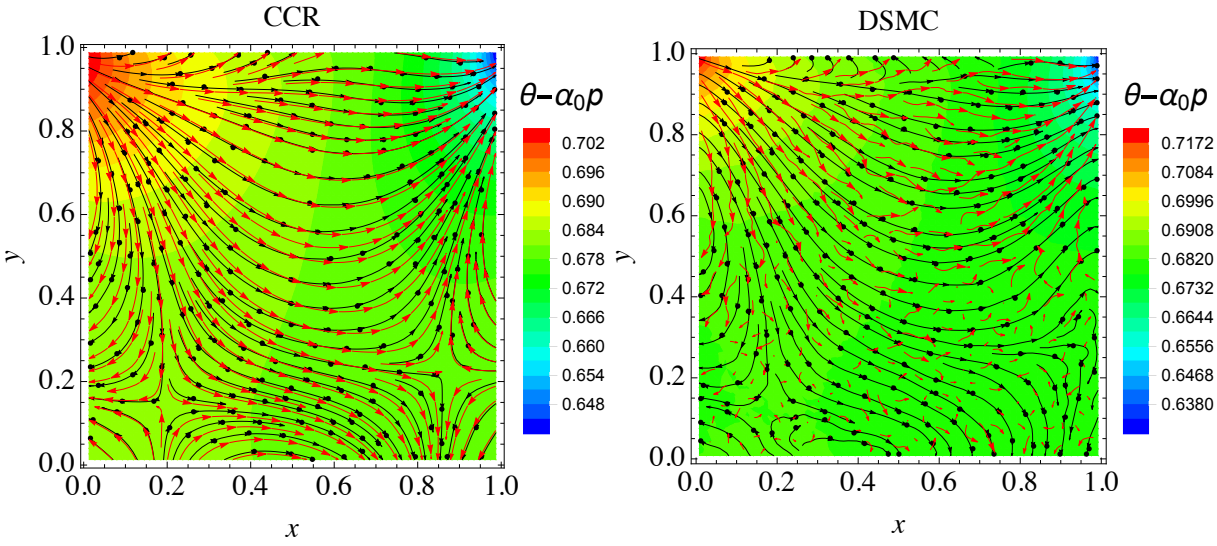

Figure 5: Heat flux lines (black) and Q_i lines (red) superimposed over temperature contours for the lid-driven cavity problem at Kn $= 0.1/\sqrt{2}$ obtained through the CCR system (left) and DSMC data (right) from [8].

6 Conclusions

Combining ideas of different approaches to Irreversible Thermodynamics, in particular LIT, RT and RET, we derived an improved set of constitutive relations for stress tensor and heat flux—the Coupled Constitutive Relations (CCR). The model describes processes in mildly rarefied gases

in sufficient approximation, and reproduces important rarefaction effects, such as the Knudsen minimum, and non-Fourier heat transfer, which cannot be described by classical hydrodynamics (NSF).

By construction, the resulting transport equations are accompanied by a proper entropy inequality with non-negative entropy generation for all processes and are linearly stable. This is a clear distinction to other models for rarefied gases, such as the Burnett equations, which are unstable due to lack of a proper entropy, or Grad-type moment equations, which are accompanied by proper entropy inequalities, and are stable, only in the linear case [15].

Thermodynamically consistent boundary conditions for the CCR system have been developed as well, which describe velocity slip, temperature jump and transpiration flow at the boundaries.

The CCR add several higher order terms to the NSF system, in bulk and at the boundary. The CCR system is accompanied by an entropy inequality, in which the entropy remains the equilibrium entropy as integrated from the equilibrium Gibbs equation, but entropy flux and entropy generation exhibit higher order correction terms. The model gives a good description of some important rarefaction effects, but does not provide as fine resolution as the full Boltzmann equation, or higher order moment equations (e.g., R13 and R26 [17, 21]). In particular, Knudsen layers are not resolved, and only appear indirectly in the corrected jump and slip coefficients.

The development of macroscopic transport equations for rarefied gases at larger orders in the Knudsen number with a full formulation of the second law of thermodynamics is an important project within the field of non-equilibrium thermodynamics. Often one will accept an approximation of the second law, if the system of equations provides sufficient accuracy for the description of processes. For instance, the regularized 13-moment (R13) equations provide good accuracy, but have a proven second law only in the linearized case. While this guarantees linear stability, little can be said about the non-linear behavior. On the other hand, cases where the full second law—linear and non-linear—is enforced, are either not amenable to analytic closure [23], or are not sufficiently accurate [47].

In steady state, the linearized CCR system reduce to the linearized Grad's 13-moment equations, which have been studied extensively in the literature. In particular, Green's functions solutions were obtained for the steady state linearized Grad equations by Lockerby and Collyer [48]. The numerical framework based upon these fundamental solutions can readily be implemented for the linearized CCR system allowing for three-dimensional steady computation at remarkably low computational cost. The appropriate numerical recipes for the nonlinear CCR system would be challenging—especially due to the non-local coupling of stress and heat flux—which will be the subject of future research.

The successful development of thermodynamically consistent transport equations for rarefied gases at higher orders will only be possible by using the best of several approaches to irreversible thermodynamics, and new ideas. We hope that the development of the CCR system based on ideas of LIT, RT and RET will be a useful step towards this end. We also envisage that these and similar ideas will prove useful for further development of recent moment models for monatomic gas mixtures [49, 50] and granular gases [51].

Acknowledgment: This work has been financially supported in the UK by EPSRC grant EP/N016602/1. ASR gratefully acknowledges the funding from the European Union's Horizon 2020 research and innovation programme under the Marie Skłodowska Curie grant agreement no. 713548. VKG gratefully acknowledges the financial support through the Commonwealth Rutherford Fellowship. HS gratefully acknowledges support through an NSERC Discovery grant.

A Decomposition of a vector and a tensor

A vector a_i and a symmetric traceless tensor A_{ij} can be decomposed into their components in the direction of a given normal $\boldsymbol{n}$ and in the directions perpendicular to it (tangential directions)

as follows. The vector a_i is decomposed as

$$a_i = a_n n_i + \bar{a}_i,$$

where $a_n n_i$ with $a_n = a_k n_k$ is the normal component of a_i while $\bar{a}_i = a_i - a_n n_i$ is the tangential component of a_i. By definition, $\bar{a}_i$ is such that $\bar{a}_i n_i = 0$.

The symmetric traceless tensor A_{ij} is decomposed as [31]

$$A_{ij} = \frac{3}{2} A_{nn}\, n_{\langle i} n_{j\rangle} + \bar{A}_{ni} n_j + \bar{A}_{nj} n_i + \tilde{A}_{ij}, \tag{43}$$

where Einstein summation never applies to the indices "n" and $A_{nn} = A_{kl} n_k n_l$. The first term in the summation of the above decomposition is the component of the tensor A_{ij} in the direction of normal; the second and third terms in the summation of the above decomposition are the normal-tangential components of A_{ij}; the fourth term in the summation of the above decomposition denotes the tangential-tangential component of A_{ij}. By definition, $\bar{A}_{nk} n_k = 0$ and $\tilde{A}_{ij} n_i = \tilde{A}_{ij} n_j = 0$. Multiplication of eq. (43) with n_j yields

$$\bar{A}_{ni} = A_{ij} n_j - A_{nn} n_i, \tag{44}$$

and eq. (43) itself gives

$$\tilde{A}_{ij} = A_{ij} - \frac{3}{2} A_{nn}\, n_{\langle i} n_{j\rangle} - \bar{A}_{ni} n_j - \bar{A}_{nj} n_i. \tag{45}$$

References

[1] Y. Sone, Kinetic Theory and Fluid Dynamics, Birkhäuser, Boston, 2002.

[2] H. Struchtrup, Macroscopic Transport Equations for Rarefied Gas Flows, Springer, Berlin, 2005.

[3] H. Struchtrup, M. Torrilhon, Higher-order effects in rarefied channel flows, Phys. Rev. E 78 (2008) 046301. doi:10.1103/PhysRevE.78.046301.

[4] A. Mohammadzadeh, A. S. Rana, H. Struchtrup, Thermal stress vs. thermal transpiration: A competition in thermally driven cavity flows, Phys. Fluids 27 (2015) 112001. doi:10.1063/1.4934624.

[5] T. Ohwada, Y. Sone, K. Aoki, Numerical analysis of the Poiseuille and thermal transpiration flows between two parallel plates on the basis of the Boltzmann equation for hard-sphere molecules, Phys. Fluids A 1 (1989) 2042–2049. doi:10.1063/1.857478.

[6] P. Taheri, M. Torrilhon, H. Struchtrup, Couette and Poiseuille microflows: Analytical solutions for regularized 13-moment equations, Phys. Fluids 21 (2009) 017102. doi:10.1063/1.3064123.

[7] A. Rana, R. Ravichandran, J. H. Park, R. S. Myong, Microscopic molecular dynamics characterization of the second-order non-Navier-Fourier constitutive laws in the Poiseuille gas flow, Phys. Fluids 28 (2016) 082003. doi:10.1063/1.4959202.

[8] B. John, X.-J. Gu, D. R. Emerson, Investigation of heat and mass transfer in a lid-driven cavity under nonequilibrium flow conditions, Num. Heat Transfer B: Fundam. 58 (2010) 287–303. doi:10.1080/10407790.2010.528737.

[9] A. Rana, M. Torrilhon, H. Struchtrup, A robust numerical method for the R13 equations of rarefied gas dynamics: Application to lid driven cavity, J. Comput. Phys. 236 (2013) 169–186. doi:10.1016/j.jcp.2012.11.023.

[10] S. R. de Groot, P. Mazur, Non-Equilibrium Thermodynamics, North-Holland, Amsterdam, 1962.

[11] S. Kjelstrup, D. Bedeaux, E. Johannessen, J. Gross, Non-Equilibrium Thermodynamics for Engineers, World Scientific, Singapore, 2010.

[12] I. Gyarmati, Non-Equilibrium Thermodynamics, Springer, Berlin, 1970.

[13] I. Müller, Thermodynamics, Pitman, Boston, 1985.

[14] B. D. Coleman, W. Noll, The thermodynamics of elastic materials with heat conduction and viscosity, Arch. Ration. Mech. Anal. 13 (1963) 167–178. doi:10.1007/BF01262690.

[15] I. Müller, T. Ruggeri, Extended Thermodynamics, Springer, Berlin, 1993.

[16] C. Cercignani, Theory and Application of the Boltzmann Equation, Scottish Academic, Edinburgh, 1975.

[17] M. Torrilhon, Modeling nonequilibrium gas flow based on moment equations, Annu. Rev. Fluid Mech. 48 (2016) 429–458. doi:10.1146/annurev-fluid-122414-034259.

[18] S. Chapman, T. G. Cowling, The Mathematical Theory of Non-Uniform Gases, Cambridge University Press, Cambridge, 1970.

[19] H. Grad, On the kinetic theory of rarefied gases, Comm. Pure Appl. Math. 2 (1949) 331–407. doi:10.1002/cpa.3160020403.

[20] H. Struchtrup, M. Torrilhon, Regularization of Grad's 13 moment equations: Derivation and linear analysis, Phys. Fluids 15 (2003) 2668–2680. doi:10.1063/1.1597472.

[21] X.-J. Gu, D. R. Emerson, A high-order moment approach for capturing non-equilibrium phenomena in the transition regime, J. Fluid Mech. 636 (2009) 177–216. doi:10.1017/S002211200900768X.

[22] W. Dreyer, Maximisation of the entropy in non-equilibrium, J. Phys. A: Math. Gen. 20 (1987) 6505–6517.

[23] J. G. McDonald, C. P. T. Groth, Towards realizable hyperbolic moment closures for viscous heat-conducting gas flows based on a maximum-entropy distribution, Continuum Mech. Thermodyn. 25 (2013) 573–603. doi:10.1007/s00161-012-0252-y.

[24] A. V. Bobylev, The Chapman-Enskog and Grad methods for solving the Boltzmann equation, Sov. Phys. Dokl. 27 (1982) 29–31.

[25] K. A. Comeaux, D. R. Chapman, R. W. MacCormack, An analysis of the Burnett equations based on the second law of thermodynamics, AIAA paper (1995) 95–0415doi:10.2514/6.1995-415.

[26] H. Struchtrup, Positivity of entropy production and phase density in the Chapman–Enskog expansion, J. Thermophys. Heat Tr. 15 (2001) 372–373. doi:10.2514/2.6618.

[27] S. Jin, M. Slemrod, Regularization of the Burnett equations via relaxation, J. Stat. Phys. 103 (2001) 1009–1033. doi:10.1023/A:1010365123288.

[28] L. H. Söderholm, Hybrid Burnett equations: A new method of stabilizing, Transp. Theory Stat. Phys. 36 (2007) 495–512. doi:10.1080/00411450701468365.

[29] A. V. Bobylev, Generalized Burnett hydrodynamics, J. Stat. Phys. 132 (2008) 569–580. doi:10.1007/s10955-008-9556-5.

[30] A. V. Bobylev, Boltzmann equation and hydrodynamics beyond Navier–Stokes, Phil. Trans. R. Soc. A 376 (2018) 20170227. doi:10.1098/rsta.2017.0227.

[31] A. S. Rana, H. Struchtrup, Thermodynamically admissible boundary conditions for the regularized 13 moment equations, Phys. Fluids 28 (2016) 027105. doi:10.1063/1.4941293.

[32] S. Paolucci, C. Paolucci, A second-order continuum theory of fluids, J. Fluid Mech. 846 (2018) 686–710. doi:10.1017/jfm.2018.291.

[33] D. Jou, G. Lebon, J. Casas-Vázquez, Extended Irreversible Thermodynamics, Springer, Netherlands, 2010.

[34] M. Slemrod, In the Chapman–Enskog expansion the Burnett coefficients satisfy the universal relation $\varpi_3 + \varpi_4 + \theta_3 = 0$, Arch. Ration. Mech. Anal. 161 (2002) 339–344. doi:10.1007/s002050100180.

[35] S. Reinecke, G. M. Kremer, Burnett's equations from a (13+9N)-field theory, Continuum Mech. Thermodyn. 8 (1996) 121–130. doi:10.1007/BF01184766.

[36] S. Kjelstrup, D. Bedeaux, Non-equlibrium Thermodynamics of Heterogeneous Systems, World Scientific, Singapore, 2008.

[37] H. Struchtrup, M. Torrilhon, H theorem, regularization, and boundary conditions for linearized 13 moment equations, Phys. Rev. Lett. 99 (2007) 014502. doi:10.1103/PhysRevLett.99.014502.

[38] J. C. Maxwell, On stresses in rarefied gases arising from inequalities of temperature, Phil. Trans. R. Soc. Lond. 170 (1879) 231–256. doi:10.1098/rstl.1879.0067.

[39] S. K. Loyalka, Velocity profile in the Knudsen layer for the Kramer's problem, Phys. Fluids 18 (1975) 1666–1669. doi:10.1063/1.861086.

[40] T. Ohwada, Y. Sone, K. Aoki, Numerical analysis of the shear and thermal creep flows of a rarefied gas over a plane wall on the basis of the linearized Boltzmann equation for hard-sphere molecules, Phys. Fluids A 1 (1989) 1588–1599. doi:10.1063/1.857304.

[41] S. K. Loyalka, Momentum and temperature-slip coefficients with arbitrary accommodation at the surface, J. Chem. Phys. 48 (1968) 5432–5436. doi:10.1063/1.1668235.

[42] Y. Sone, T. Ohwada, K. Aoki, Temperature jump and Knudsen layer in a rarefied gas over a plane wall: Numerical analysis of the linearized Boltzmann equation for hard-sphere molecules, Phys. Fluids A 1 (1989) 363–370. doi:10.1063/1.857457.

[43] A. Mohammadzadeh, A. Rana, H. Struchtrup, DSMC and R13 modeling of the adiabatic surface, Int. J. Therm. Sci. 101 (2016) 9–23. doi:10.1016/j.ijthermalsci.2015.10.007.

[44] C. Cercignani, S. Lorenzani, Variational derivation of second-order slip coefficients on the basis of the Boltzmann equation for hard-sphere molecules, Phys. Fluids 22 (2010) 062004. doi:10.1063/1.3435343.

[45] S. Naris, D. Valougeorgis, The driven cavity flow over the whole range of the Knudsen number, Phys. Fluids 17 (2005) 097106. doi:10.1063/1.2047549.

[46] A. Mohammadzadeh, E. Roohi, H. Niazmand, S. Stefanov, R. S. Myong, Thermal and second-law analysis of a micro- or nanocavity using direct-simulation Monte Carlo, Phys. Rev. E 85 (2012) 056310. doi:10.1103/PhysRevE.85.056310.

[47] M. Torrilhon, H-theorem for nonlinear regularized 13-moment equations in kinetic gas theory, Kinet. Relat. Models 5 (2012) 185–201. doi:10.3934/krm.2012.5.185.

[48] D. A. Lockerby, B. Collyer, Fundamental solutions to moment equations for the simulation of microscale gas flows, J. Fluid Mech. 806 (2016) 413–436. doi:10.1017/jfm.2016.606.

[49] V. K. Gupta, M. Torrilhon, Higher order moment equations for rarefied gas mixtures, Proc. R. Soc. A 471 (2015) 20140754. doi:10.1098/rspa.2014.0754.

[50] V. K. Gupta, H. Struchtrup, M. Torrilhon, Regularized moment equations for binary gas mixtures: Derivation and linear analysis, Phys. Fluids 28 (2016) 042003. doi:10.1063/1.4945655.

[51] V. K. Gupta, P. Shukla, M. Torrilhon, Higher-order moment theories for dilute granular gases of smooth hard spheres, J. Fluid Mech. 836 (2018) 451–501. doi:10.1017/jfm.2017.806.